ISSN 1070-4272, Russian Journal of Applied Chemistry © Pleiades Publishing, Ltd., 2024.

CATALYSIS

Influence of the Silicon Deposition on the Industrial Silicon Trapping Catalyst

Xiaozhen Chen[a,*], Li Liu[a,], Chengmin Yang[a], Bumei Zheng[a], Xiaoying Yin[a], Jin Sun[a], Yunhai Yao[a], and Weiyu Duan[a]**

[a] *SINOPEC (Dalian) Research Institute of Petroleum and Petrochemicals Co., Ltd., Dalian, 116045 China*
**e-mail: chenxiaozhen.fshy@sinopec.com*
***e-mail: liuli.fshy@sinopec.com*

Received August 4, 2023; revised February 5, 2024; accepted February 5, 2024

Abstract—The structure and surface properties of the industrial silicon trapping catalysts were characterized by XRF, XPS, XRD, NH_3-TPD and NMR. The silicon trapping mechanism of the industrial silicon trapping catalyst was discussed. The results showed that the silicon capacity reached 28.17% during this lifetime. The captured silicon mainly existed on the surface of the silicon trapping catalyst as amorphous silicon with abundant Q species including $Si(OSi)_4$, $Si(OSi)_3(OX)$, $Si(OSi)_2(OX)_2$, and $Si(OSi)(OX)_3$, proving the silicon was caputured as the amorphous silicon bilayer deposition model. After silicon deposition, the pore properties of the silicon trapping catalyst changed greatly. Compared with the fresh catalyst, the specific surface area and pore volume of the spent industrial silicon trapping catalyst decreased by 49.17% and 22.92% respectively. The deposition of silicon leaded to the loss of acid sites and changed the interaction between the support and the active metal, which result in the reduction of the number of active metal species. This may explain how the deposited silicon is related to the deactivation of the hydrotreating catalysts.

Keywords: industrial silicon trapping catalyst, deactivation, surface properties, Q species

DOI: 10.1134/S1070427224020071

ABBREVIATIONS AND NOTATION

XRF, X-ray fluorescence; XPS, X-ray photoelectron spectroscopy; XRD, X-ray diffraction; NMR, Nuclear magnetic resonance spectroscopy; FHRS-2, the industrial silicon trapping catalyst; FS-Spent, the spent FHRS-2; FS-Fresh, the Fresh FHRS-2; FS-Spent-500, the sample obtained by calcinating FS-Spent at 500°Cfor 3 h in air atmosphere; w, silicon capacity; M_{SiO2}, the content of SiO_2 in the catalysts FS-Spent-500; M_0, the initial mass of the silicon trapping catalysts.

INTRODUCTION

Antifoaming containing organosilicon is often used in the coke drums, which will lead to the generation of light silicon compounds in the light components. This part of silicon will affect the deactivation of the hydrotreating catalysts. Recently, researchers have studied the process of Si-poisoned catalysts and the application of silicon trapping catalysts. Pérez-Romo and his groups studied the species of silicon on the deactivated catalyst and proposed that the silicon on the deactivated hydrogenation catalyst mainly existed in the form of SiO_2 with Si(OH), $Si(OH)_2$, $\equiv SiCH_3$, $SiOHCH_3$ and $Si(CH_3)_2$ groups [1]. Vatutina et al. explored the regeneration possibility of Si-poisoned hydrotreating catalysts $CoMo/Al_2O_3$. The spent catalysts with different silicon contents were regenerated and then activated by citric acid. The results showed that the hydrodesulfurization activity of the regenerated $CoMo/Al_2O_3$ catalysts decreased with the increase of silicon content. The hydrodesulfurization activity of the regenerant catalysts could be recovered, when the silicon content on $CoMo/Al_2O_3$ was less than 3%. In addition, they also proposed that the increase of silicon content on the deactivated catalysts led to the increase

of CoO_x species on the regenerant catalysts. The Co species could not be converted into active Co species during the sulphur treatment, and could not effectively modify MoS_2 layers, which resulted in the decrease of the hydrodesulfurization activity of the corresponding regenerant catalysts [2].

There were some silicon trapping catalysts has been developed as the protectant for the capture of silicon. Qu studied the application of silicon-trapping catalysts in the coking gasoline hydro-processing unit. It was found that FHRS-1 developed by Fushun Petrochemical Research Institute showed the characteristics of large pore volume, large specific surface area and high silicon capacity [3]. Chen analyzed the deactivation of the HPS-02A and HPS-02B silicon trapping catalysts in the coking diesel hydrogenation unit, and studied the deactivation degree of the silicon trapping catalysts at different positions of the unit. The results showed that the silicon content of the silicon trapping catalysts gradually decreased along the direction of material flow from top to bottom. In addition, the silicon trapping catalysts showed the performance of hydrogenation and deferrization of raw materials. The properties of reclaimed silicon-trapping catalysts indicated that deposition deactivation of impurities such as silicon and iron is irreversible [4].

There are few reports about the industrial silicon trapping catalysts and the influence of the silicon on the NiMo type silicon-trapping catalysts. In order to provide support for the research of the silicon trapping mechanism of industrial silicon trapping catalysts and the deactivation mechanism of NiMo type silicon-trapping catalysts deriving from silicon deposition, the study made an in-depth analysis of the microstructure properties, surface active phase properties, acid properties and silicon species on the surface of the industrial silicon-trapping catalysts.

EXPERIMENTAL

Preparation of materials. The spent and the fresh industrial silicon trapping catalysts used in the experiment was the FHRS-2 from the industrial unit of a refinery. The spent FHRS-2 marked as FS-Spent was used to trap silicon for one cycle in naphtha hydrogenation unit. Fresh catalyst FHRS-2 was labelled as FS-Fresh. The sample named as FS-Spent-500 was obtained by calcinating FS-Spent at 500°Cfor 3 h in air atmosphere.

Characterization of catalysts. The pore properties of the samples were analysed by Nitrogen physical adsorption. The analytical instrument was ASAP 2420 nitrogen physical adsorption instrument from MICROMERITICS Corporation. The samples were vacuumized and pre-treated at 200°C for 4 h.

The surface metal species were characterized by XPS. Prior to XPS testing, the samples were pre-sulfureted in $10\%H_2S/H_2$ mixture. The pre-treated catalyst was characterized by XPS analysis on MULTILAB2000 XPS of VG Scientific Instruments. In the test, MgK_α target was used as the excitation source, Al2p spectral peak was used as the internal standard, and the test pressure was less than 5×10^{-8} Pa. The sample is supported with conductive scotch tape.

The Si and Al species information of the samples were obtained by NMR analysis. The analytical instrument was Bruker BioSpin GmbH from Germany, which has a probe of 4 mm MAS BB/1H H7999/0017. The instrument frequency is 130.32MHZ, and deuterobenzene is the solvent.

The phase composition of the samples was analyzed by XRD. The instrument is D/Max-2500X-ray diffractometer of RIGAKU Company of Japan. The light source is CuK_α ray, the voltage is 20~60 kV, and the current is 10~300 mA. The scan range is from 10° to 70°, step size is 0.01°, and scan rate is 1°/min. The sample was pulverized and pressed before testing.

The acid properties of the samples were characterized by NH_3-TPD. The samples were saturated with NH_3 at 100°C for 1h, and then after being purged with pure He for 2 h at the same temperature, the samples were heated at 10 °C min^{-1} to 773 K under He flow. The instrument is AutoChem 2920 automatic chemisorption instrument of Mack Instrument Company. Bluer XRF instrument is used to test the silicon content of the samples. Before the test, the samples were pretreated at 500°C for 3 h in the air atmosphere.

The mass content of SiO_2 in the catalysts is M_{SiO_2},

$$M_{SiO_2} = M_1 S \quad (1)$$

Thereinto, S is the mass content of SiO_2 in the used samples after treated at 500°C measured by the XRF anlysis, M_1 is the mass of the used samples after treated at 500°C.

w presents silicon capacity, %:

Table 1. The texture properties of the silicon trapping catalysts

Samples	S_{BET}, $m^2 g^{-1}$	V_P, $cm^3 g^{-1}$	D, nm	SiO_2, wt %	Si capacity, %
FS-Fresh	303	0.48	6.4	–	28.17
FS-Spent-500	154	0.37	9.6	21.98	

$$w = \frac{M_{SiO_2}}{M_0} \times 100, \quad (2)$$

Thereinto, M_0 stands for the initial mass of the silicon trapping catalysts.

RESULTS AND DISCUSSION

The physicochemical properties of the silicon trapping catalysts. The phase information of the samples could be obtained by XRD. Figure 1 showed the XRD analysis results of FS-Fresh and FS-Spent-500. It could be seen from Fig. 1 that FS-Fresh exhibited an apparent diffraction peak of γ-Al_2O_3, and there was no NiO or MoO_3 diffraction peaks was found. It could be likely that the particle size of the active metal components on FS-Fresh was very small and the particles were evenly dispersed, which probably led to the results that only the diffraction peaks of supports were detected. Compared with the obvious diffraction peaks of the supports of FS-Fresh, the position of the diffraction peaks of FS-Spent-500 does not change significantly, but the peaks intensity of the support decreased significantly. It was apparent that the support was mainly consisted of γ-Al_2O_3 after calcination, while the deposition of silicon on the surface of the silicon trapping catalyst caused the change of surface phase composition of the FS-Spent-500, which resulted in the decreaγsing of the peak strength of the support FS-Spent-500 greatly. The result demonstrated that the silicon deposited on the surface of the silicon trapping catalyst reacted with the γ-Al_2O_3 support, which would affect the properties of the silicon trapping catalyst.

In order to explore the effect of silicon deposition on the structural properties of the silicon trapping catalysts, the pore structure of silicon trapping catalysts was analyzed by nitrogen physical adsorption. Figure 2 presented the pore properties of the FS-Fresh and FS-Spent-500, where Fig. 2b exhibited the corresponding pore size distribution and Fig. 2a showed the adsorption isotherms. It could be seen from the adsorption isotherm curves of FS-Fresh and FS-Spent-500 that both fresh and the calcinated spent catalysts belonged to mesoporous materials, even though there were some differences in pore structure [5]. As shown in Fig. 2a, it could be seen that the pore size distribution of the silicon trapping catalysts under different states was quite different. The pore size distribution of FS-Fresh is relatively concentrated, where the average pore size is 6.4 nm. However, the average pore size of FS-Spent-500 is 9.6 nm. It is observed that the deposited silicon changed the pore structure of the catalysts. In addition, he pore size distribution of FS-Spent-500 was relatively dispersed. The number of pores smaller than 10nm was greatly reduced, while many mesoporous pores with pore size around 25 nm were increased. And as shown in Fig. 2b, the adsorption isotherms of FS-Spent-500 is a little different with that of FS-Fresh, which was related to the change of the pore shape and also presented the pore structure was changed. As exhibited in Table 1, the specific surface area and pore volume of the silicon trapping catalysts decreased significantly after silicon deposition. Compared with the FS-Fresh the specific surface area and pore volume of FS-Spent-500 decreased by 49.17 and 22.92%, respectively. In summary, the pore property analysis proved that silicon deposition made the specific surface area and pore volume decreased. The silicon deposited on the surface of the silicon trapping catalysts caused

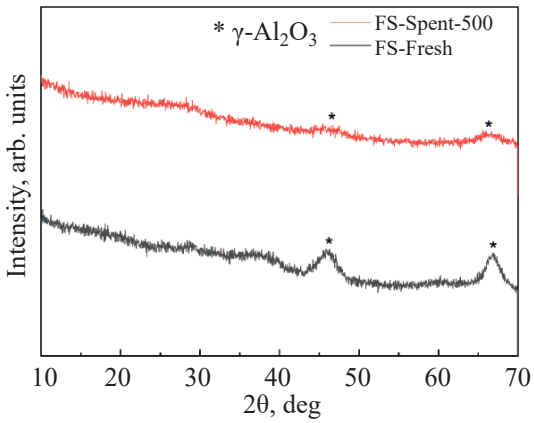

Fig. 1. The XRD patterns of the silicon trapping catalysts.

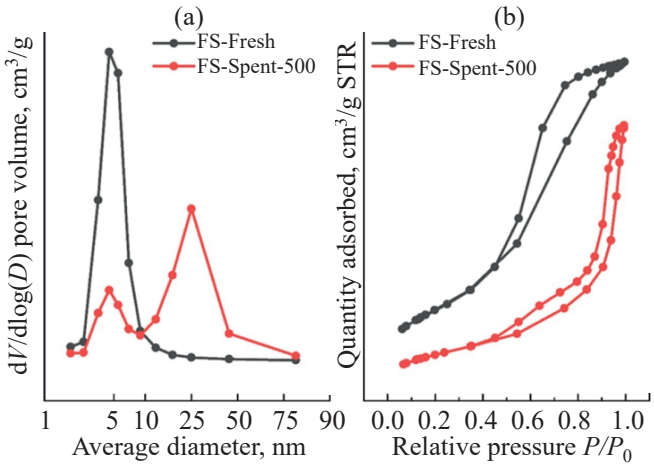

Fig. 2. The pore properties of the silicon trapping catalysts.

the blocking of the pores with different sizes, resulting in the change of the pore structure of silicon trapping catalysts. The activity of catalyst is closely related to the properties of pores, and the change of pore structure would affect the adsorption and diffusion of reactant molecules, which ultimately leads to the loss of catalyst performance [6]. In addition, the silicon captured by silicon trapping catalyst was characterized by XRF. As shown in Table 1, there was 21.98 wt.% SiO_2 detected by XRF over FS-Spent-500, by which the Si capacity of FHRS-2 could be obtained. Combined with Eq. (1), the Si capacity of FHRS-2 is 28.17% shown in Table 1.

The surface properties of the silicon trapping catalysts. Figure 3 exhibited the NH_3-TPD spectra of FS-Fresh and FS-Spent-500, where the surface acid properties of silicon trapping catalysts could be obtained. As demonstrated in Fig. 3, the NH_3 adsorption peak strength of FS-Spent-500 was much weaker than

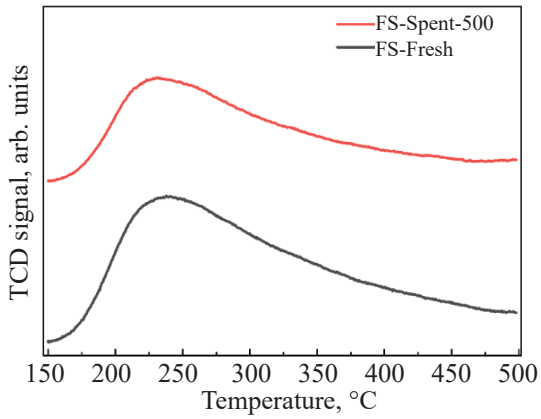

Fig. 3. The NH_3-TPD of the silicon trapping catalysts.

that of FS-Fresh, proving that the deposition of silicon on the surface of the silicon trapping catalysts made the change of the acid centers [6]. The total acid content of FS-Fresh and FS-Spent-500 were 0.401mmol/g and 0.343mmol/g, respectively according to the results analyzed from Fig. 3. Compared with FS-Fresh, the total acid content of FS-Spent-500 was reduced by 14.46%. This result presented that the deposited silicon could cover the acid center on the catalyst, resulting in the reduction of the acid center. According to the literature, the acid center is related to the activity of hydrogenation catalyst, and the reduction of acid center will also cause the loss of the catalytic activity.

In order to clarify the surface properties of the industrial silicon trapping catalysts, analyze the structure and composition of silicon on the industrial silicon trapping catalysts, NMR analysis was carried out to study the species of silicon. Figure 4 showed ^{29}Si NMR spectra of FS-Spent and FS-Spent-500, where the silicon species deposited on their surface were analyzed. Kellberg analyzed the catalysts for silicon poisoning from coking gasoline hydrogenation by combining ^{29}Si MAS and ^{29}Si CP/MAS methods, and found that the signal peak within the chemical shift between –14 and –22.4 ppm belonged to the D species (=Si($(CH_3)_2$) with two methyl groups. The two peaks at –54 and –64 ppm were attributed to the T species (≡$SiCH_3$) with one methyl group, while the three overlapping peaks between –85 and –120 ppm were attributed to the Q species with the siloxy group (Q: Si(OX), where X is H, Al or Si) [7]. Based on existing studies, it can be concluded that Q species can

be divided into four categories: $Si(OSi)_4$ (~112 ppm), $Si(OSi)_3(OX)$ (~103 ppm), $Si(OSi)_2(OX)_2$ (~93 ppm), $Si(OSi)(OX)_3$ (~85 ppm) [5].

As shown in Figure 4, there was only one signal peak in the ^{29}Si NMR spectra for both FS-Spent and FS-Spent-500, both of which was located between –70 and –120 ppm. The results showed that after the usage of the industrial silicon trapping catalysts for one cycle, the types of silicon species on FS-Fresh and FS-Spent-500 were same, that is, the silicon on the surface of FS-Fresh and FS-Spent-500 were mainly full of the siloxy group Si(OX) (X was H, Al or Si). Nevertheless, although the chemical shift interval of silicon species on the surface of FS-Spent and FS-Spent-500 was the same, the shape of their signal peaks was slightly different. Considering the kinds of Q species, there were differences in the distribution of silicon with different Q species on the surface of FS-Fresh and FS-Spent-500 Therefore, the ^{29}Si NMR spectra of FS-Spent and FS-Spent-500 were processed by peak splitting. As can be seen from the peak splitting results, the silicon on FS-Spent and FS-Spent-500 surfaces was Q species with abundant $Si(OSi)_4$, $Si(OSi)_3(OX)$, $Si(OSi)_2(OX)_2$, $Si(OSi)_2$, $Si(OSi)(OX)_3$ groups [5, 8]. Table 2 indicated the peak splitting results of FS-Spent and FS-Spent-500 ^{29}Si NMR spectra, and presented the surface composition of different silicon trapping catalysts. As exhibited in Table 2, the silicon distribution of the Q species on FS-Spent surface was 18.6%$Si(OSi)_4$, 47.8%$Si(OSi)_3(OX)$, 23.8%$Si(OSi)_2(OX)_2$ and 9.8%$Si(OSi)(OX)_3$. As to FS-Spent-500, the silicon distribution of Q species changed, and became 16.6%$Si(OSi)_4$, 66.0%$Si(OSi)_3(OX)$, 12.1%$Si(OSi)_2(OX)_2$ and 5.4%$Si(OSi)(OX)_3$. After high temperature regeneration treatment, the surface silicon species of FS-Spent changed, the $Si(OSi)_2(OX)_2$, $Si(OSi)_4$ and $Si(OSi)(OX)_3$ species were reduced and converted to $Si(OSi)_3(OX)$ species. This result proved that at high temperature, some bonds in siloxy groups broke and recombined, where the surface siloxy group interacted with the support were transformed into OX groups accompanied by the generation of more O–Si–O–Si groups, and finally resulting in the generation of more $Si(OSi)_3(OX)$ groups. The presence of $Si(OSi)_4$ groups with the chemical shift of –112~–109 ppm indicated that the deposition of silicon on the industrial silicon trapping catalysts did not accord with the model

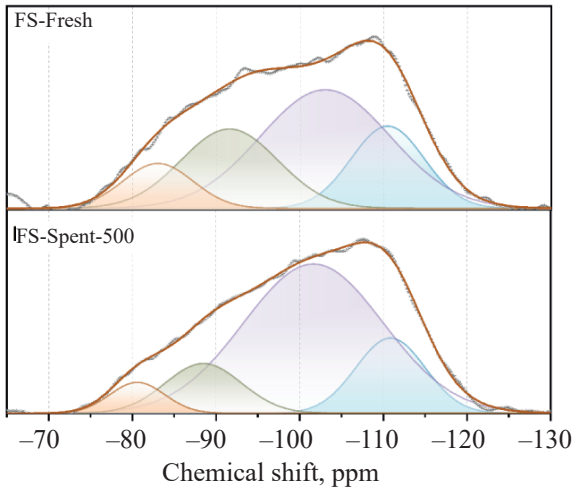

Fig. 4. ^{29}Si NMR of the silicon trapping catalysts.

of monolayer silicon deposition, where there is no pure Si–O–Si bond as $Si(OSi)_4$ groups and every silicon was believed to bond with Al. The appearance of silicon vibration at this chemical shift indicated that the silicon deposition on the silicon trapping catalyst conformed to the amorphous silicon bilayer deposition model. The formation process of amorphous silicon on the support-alumina was spontaneous, and the amorphous silicon formed by bilayer deposition model was relatively stable [8, 9, 10].

Combined the reports and ^{29}Si NMR analysis of the industrial silicon trapping catalysts, it was likely that the silicon trapping catalyst located above the bed reacted with the cyclosiloxane in the feed, where the silicon in the cyclosiloxane was finally captured by the support of the silicon trapping catalysts in the way of siloxy group, and then the amorphous silicon with Q-type silicoxy group

Table 2. The NMR results of the silicon trapping catalysts

Chemical shift, ppm	Si species	Percentage of Si species / %	
		FS-Spent	FS-Spent-500
–112~–109	$Si(OSi)_4$	18.6	16.6
–104~–101	$Si(OSi)_3(OX)$	47.8	66.0
–95~–90	$Si(OSi)_2(OX)_2$	23.8	12.1
–87~–83	$Si(OSi)(OX)_3$	9.8	5.4

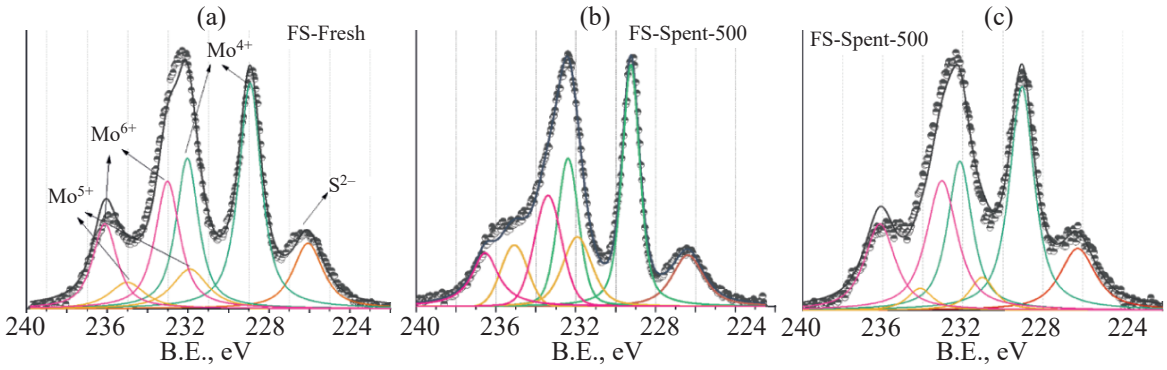

Fig. 5. Mo3d XPS of the silicon trapping catalysts.

was generated on the surface of the silicon trapping catalysts. In addition, this result also demonstrated that the silicon deposited on alumina existed in the form of amorphous silicon [9, 11, 12]. The results were also consistent with XRD results. A large amount of silicon was deposited on the surface of the silicon trapping catalysts and the coverage of amorphous siloxy structures led to a significant weakening of the X-ray diffraction peak intensity of the support alumina of FS-Spent-500. At the same time, the abnormal pore size distribution of FS-Spent-500 could be also explained. A large amount of silicon covered or blocked the pores, resulting in a significant reduction in the specific surface area and pore volume of FS-Spent-500. Meanwhile, the amorphous silicon on FS-Spent-500 might be the reason for the appearance of some bigger mesopores about 25 nm. To sum up, after the silicon in the feed was captured by the silicon trapping catalyst, the silicon was deposited on the silicon trapping catalyst in the form of amorphous siloxy groups, which blocked the pores and changed the pore properties of the silicon trapping catalyst. Meanwhile, the existence of many Q-type silicoxy groups on the surface caused the chaos of the functional groups on the surface of the silicon trapping catalyst and finally changed its surface properties including acid properties [6].

Figure 5 exhibited the Mo_{3d} XPS of FS-Fresh, FS-Fresh-500 and FS-Spent-500. The XPS characterization of the active metals in the silicon trapping catalysts can be used to clarify the active metal species on the surface of the catalysts, which was helpful to further analyze the influence of the process of silicon trapping on the surface-active phase of the silicon trapping catalysts. As shown in Fig. 5, the peaks of the Mo_{3d} spectra of FS-Fresh, FS-Fresh-500 and FS-Spent-500 were similar, indicating that the surface Mo species were similar. Nevertheless, the content of Mo species in different valence states on the silicon trapping catalysts was slightly different according to the results of peak fitting. The peak fitting rules were as follows: the difference of binding energy between $Mo_{3d3/2}$ and $Mo_{3d5/2}$ orbits is between 3.1 and 3.2 eV, and the peak area ratio between $Mo_{3d3/2}$ and $Mo_{3d5/2}$ is 2 : 3 [13, 14]. It was evident that Mo^{4+} is the Mo species in MoS_2 phase, that is, Mo^{4+} presented the Mo species in sulfide state, Mo^{5+} belonged to the Mo species in MoO_xS_y phase, while Mo^{6+} corresponded to the Mo species in MoO_3 [14, 15, 16]. Table 3 indicated the peak fitting results of XPS, and it was obvious that the distribution of Mo species in different valence states in FS-Fresh was 60.64%Mo^{4+}, 16.86%Mo^{5+} and 23.90%Mo^{6+}. What is noteworthy is that the distribution of Mo species in different valence states of FS-Spent-500 was 53.35%Mo^{4+}, 8.05%Mo^{5+} and 38.70%Mo^{6+}. In addition, the distribution of Mo species in different valence states in FS-Fresh-500 was 59.61%Mo^{4+}, 13.36%Mo^{5+}, and 27.03%Mo^{6+}. It was evident that FS-Fresh-500 owned lower Mo^{4+} species than FS-Fresh, which indicated that calcination process had an impact on the sulfidity of the catalysts. The Mo^{4+} species of FS-Spent-500 decreased by 12.02% compared with FS-Fresh and 10.50% compared with FS-Fresh-500, which indicated that the deposition of silicon also resulted in the decrease of sulfidity of the used silicon-trapping catalyst. The possible reason was that the interaction between the deposited silicon on the surface and the support brought about the limited sulphuration of active metals and the decrease of the number of

Table 3. The active species (XPS) of the silicon trapping catalysts

Samples	Mo^{4+}	Mo^{5+}	Mo^{6+}	NiS_x	Ni–Mo–S	Ni^{2+}
FS-Fresh	60.64	16.86	23.90	11.26	42.82	45.92
FS-Fresh-500	59.61	13.36	27.03	14.33	38.30	49.37
FS-Spent-500	53.35	8.05	38.70	12.88	31.79	55.33

active phases. This was one of the important reasons for the loss of catalyst activity. Figure 6 exhibited the Ni_{2P} XPS spectra of FS-Spent-500 and FS-Fresh. The peak fitting rules were as follows: the difference of binding energy between $Ni_{2p3/2}$ and $Mo_{2p1/2}$ orbits is 17.3 eV, and the peak area ratio between Ni $_{2p3/2}$ and $Mo_{2p1/2}$ is 2 : 1. It is apparent that Ni in the silicon trapping catalysts mainly existed in three forms: Ni_{NiSx}, $Ni_{Ni–Mo–S}$ and Ni^{2+} species. Thereinto, the Ni^{2+} species was the Ni species in the oxidation state in NiO or $NiAlO_4$ phase [14, 16]. The contents of different species of Ni in FS-Spent-500, FS-Fresh and FS-Fresh were listed in Table 3. Obviously, the content of $Ni_{Ni–Mo–S}$ species in FS-Spent-500 was 31.79%. Nevertheless, the content of $Ni_{Ni–Mo–S}$ species in FS-Fresh was 42.82%, FS-Fresh-500 owned 38.30%$Ni_{Ni–Mo–S}$ species. FS-Fresh-500 showed lower $Ni_{Ni–Mo–S}$ species than FS-Fresh, indicating that the calcination would also influence the modification of Mo by Ni and decrease the content of Ni–Mo–S species. However, the content of active $Ni_{Ni–Mo–S}$ species in FS-Spent-500 decreased by 25.76% compared with FS-Fresh and 17.00% compared with FS-Fresh-500, which means that the Si deposition might also affect the formation of $Ni_{Ni–Mo–S}$ species and decrease the sulfidity of Ni in the catalysts. This result proved that the deposition of silicon on the surface of the silicon trapping catalysts could impede the activation process of active metal Ni, which could not modify MoS_2 species effectively and resulted in a decrease in the number of active $Ni_{Ni–Mo–S}$ species. Finally, the number of highly active NiMoS active phase was reduced, leading to the decrease of catalyst hydrodesulfurization performance [15].

To sum up, it can be speculated that the interaction between deposited silicon on the surface of the silicon trapping catalysts and the support changed the structural and surface properties of the silicon trapping catalysts, resulting in the reduction of the sulfidity of the active metals during the activation of the used catalyst, and the weakening of the effective modification of MoS_2 species by Ni. Thus, the hydrodesulfurization performance of the catalyst was reduced.

CONCLUSIONS

It can be concluded that the silicon capacity of FHRS-2 was as high as 28.17% in the industrial device during the operation cycle. It could be found that the silicon deposition on the silicon trapping catalysts from industrial devices conformed to the amorphous silicon bilayer deposition model, where the silicon mainly existed in the form of amorphous silicon with

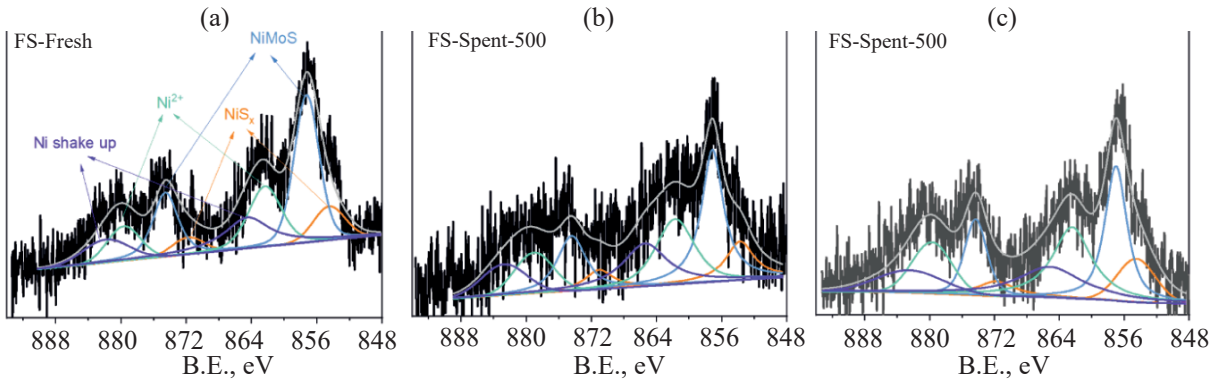

Fig. 6. Ni2P XPS of the silicon trapping catalysts.

abundant Q species including $Si(OSi)_4$, $Si(OSi)_3(OX)$, $Si(OSi)_2(OX)_2$, $Si(OSi)(OX)_3$ (X=H, Si, Al) groups.

Silicon deposition has a great influence on the structural properties of the silicon trapping catalysts. The deposited silicon existed in amorphous structure on the surface of the silicon trapping catalysts, resulting in the change or blockage of many pores and a significant reduction of specific surface area and pore volume. The specific surface area and pore volume of FS-Spent-500 were reduced by 49.17 and 22.92% compared with FS-Fresh, respectively. In addition, the surface amorphous silicon made the pore distribution of the catalysts after silicon deposition disorganized and dispersed, which was not conducive to the adsorption, diffusion, and reaction of the molecules during the hydrogenation, and was one of the important reasons for the loss of catalyst activity.

After silicon deposition, the surface acid content of FS-Spent-500 decreased by 14.46% compared with FS-Fresh, while the surface active Mo^{4+} species and $Ni_{Ni–Mo–S}$ species of FS-Spent-500 decreased by 12.02% and 25.76%, respectively. The silicon deposited on the surface covered the surface of the silicon trapping catalyst, which resulted in the loss of acid sites and changed the interaction between the support and the active metal by reacting with the support. Therefore, the deposited silicon inhibited the sulphuration of the active metals to some extent, reducing the sulfidity of the active metals, and greatly weakening the modification effect of the active metal Ni on the active phase of MoS_2. Thus, the production of highly active NiMoS phase was reduced, which was another important reason for catalyst deactivation after regeneration.

ADDITIONAL INFORMATION

Xiaozhen Chen, ORCID: https://orcid.org/0000-0002-0413-1695

FUNDING

We gratefully acknowledge financial support provided by the Liaoning Revitalization Talent Program under Grant XLYC2002102 and Dalian High-level Innovation and Entrepreneurship Program under Grant 2020RD10.

CONFLICT OF INTEREST

The authors declare no conflict of interest.

REFERENCES

1. Pérez-Romo, P., Aguilar-Barrera, C., Laredo, G.C., Ángeles-Chávez, C., and Fripiat, J., *Applied Catalysis A: General.*, 2021, vol. 611, p. 117964. https://doi.org/ 10.1016/j.apcata.2020.117964
2. Vatutina, Y.V., Kazakov, M.O., Nadeina, K.A., Budukva, S.V., Danilova, I.G., Gerasimov, E.Y., Suprun, E.A., Prosvirin, I.P., Nikolaeva, O.A., Gabrienko, A.A., Klimov, O.V., Noskov, A.S., *Catalysis Today*, 2021, vol. 378, pp. 43–56. https://doi.org/10.1016/j.cattod.2021.03.005
3. Qu, T., Jia, B.J., Chai, H., Guo, R., *Petroleum Refinery Engineering,* 2009, vol. 39, p. 47–49. https://doi.org/10.3969/j.issn.1002-106X.2009.10.012
4. Chen, Y.F., Xin, J., Han, N.L., Liu, X.C., Wang, L.Y., and Song, Y., *Speciality Petrochemicals*, 2021, vol. 38, pp. 34–38. https://doi.org/10.3969/j.issn.1003-9384.2021.05.008
5. Pérez-Romo, P., Navarrete-Bolaños, J., Aguilar-Barrera, C., Angeles-Chavez, C., and Laredo, G.C., *Applied Catalysis A: General,* 2014, vol. 485, p. 84–90. https://doi.org/10.1016/j.apcata.2014.07.038
6. Nadeina, K.A., Kazakov, M.O., Kovalskaya, A.A., Danilova, I.G., Cherepanova, S.V., Danilevich, V.V., Gerasimov E.Yu., Prosvirin I.P., Kondrashev A.V., Klimov, O.V., Noskov A. S., *Catalysis Today*, 2020, vol. 353, pp. 53–62. https://doi.org/10.1016/j.cattod.2019.10.028
7. Kellberg, L., Zeuthen, P., and Jakobsen, H.J., *Journal of Catalysis*, 1993, vol. 143, pp. 45–51. https://doi.org/10.1006/jcat.1993.1252
8. Vaiss, V.S., Fonseca, C.G., Antunes, F.P.N., Chinelatto, L.S.Jr., Chiaro, S.S.X., Souza, W.F., and Leitão, A.A., *J. Catalysis,* 2020, vol. 389, pp. 578–591.
9. Caillot, M., Chaumonnot, A., Digne, M., and Bokhoven, J.A.V., *ChemCatChem,* 2013, vol. 5, pp. 3644–3656. https://doi.org/10.1002/cctc.201300560
10. Caillot, M., Chaumonnot, A., Digne, M., Poleunis, C., Debecker, D.P., and van Bokhoven, J.A., *Microporous and Mesoporous Materials,* 2014, vol. 185, pp. 179–189. https://doi.org/10.1016/j.micromeso.2013.10.032
11. Thomas, J.M., *Microporous and Mesoporous Materials,* 2007, vol. 104, pp. 5–9. https://doi.org/10.1016/j.micromeso.2007.01.002
12. Pérez-Romo, P., Aguilar-Barrera, C., Navarrete-

Bolaños, J., Rodríguez-Otal, L.M., Beltrán, F.H., and Fripiat, J., *Applied Catalysis A: General*, 2012, vol. 449, pp. 183–187. https://doi.org/10.1016/j.apcata.2012.10.001

13. Li, Y., Zhang, T., Liu, D., Liu, B., Lu, Y., Chai, Y., and Liu C.G., *Industrial & Engineering Chemistry Research,* 2019, vol. 58, pp. 17195–17206. https://doi.org/10.1021/acs.iecr.9b02368
14. Hu, D., Li, H.P., Mei, J.L., Xiao, C.K., Wang, E.H., Chen, X.Y., Zhang W.X., and Duan A.J., *Petroleum Science,* 2022, vol. 19, pp. 321–328. https://doi.org/10.1016/j.petsci.2021.11.005
15. Kobayashi, K., Nagai, M., *Catalysis Today*, 2017, vol. 292, pp. 74–83. https://doi.org/10.1016/j.cattod.2017.01.040
16. Liu, Z.W., Han, W., Hu, D.W., Sun, S.L., Hu, A.P, Wang, Z., Jia, Y.Z., Zhao, X.Q., and Yang, Q.H., *J. Catalysis,* 2020, vol. 387, pp. 62–72. https://doi.org/10.1016/j.jcat.2020.04.008